On the benefit of smart tyre technology on vehicle state estimation

Taylor & Francis
Taylor & Francis Group

Vehicle System Dynamics
International Journal of Vehicle Mechanics and Mobility

ISSN: (Print) (Online) Journal homepage: www.tandfonline.com/journals/nvsd20

On the benefit of smart tyre technology on vehicle state estimation

Victor Mazzilli, Davide Ivone, Stefano De Pinto, Leonardo Pascali, Michele Contrino, Giulio Tarquinio, Patrick Gruber & Aldo Sorniotti

To cite this article: Victor Mazzilli, Davide Ivone, Stefano De Pinto, Leonardo Pascali, Michele Contrino, Giulio Tarquinio, Patrick Gruber & Aldo Sorniotti (2022) On the benefit of smart tyre technology on vehicle state estimation, Vehicle System Dynamics, 60:11, 3694-3719, DOI: 10.1080/00423114.2021.1976414

To link to this article: https://doi.org/10.1080/00423114.2021.1976414

Published online: 24 Oct 2021.

VEHICLE SYSTEM DYNAMICS
2022, VOL. 60, NO. 11, 3694–3719
https://doi.org/10.1080/00423114.2021.1976414

On the benefit of smart tyre technology on vehicle state estimation

Victor Mazzilli[a], Davide Ivone[b], Stefano De Pinto[c], Leonardo Pascali[c], Michele Contrino[c], Giulio Tarquinio[c], Patrick Gruber [a] and Aldo Sorniotti [a]

[a]Department of Mechanical Engineering Sciences, University of Surrey, Guildford, UK; [b]Pirelli Tyre S.p.A., Milan, Italy; [c]McLaren Automotive Limited, McLaren Technology Centre, Woking, UK

ABSTRACT

Among other variables, smart tyre systems are capable of determining tyre contact forces. Combining this information with the signals obtained from conventional vehicle sensors, e.g. inertial measurement units, wheel speed sensors and steering wheel angle sensors, improves the estimation accuracy of the states used by the vehicle dynamics controllers of production cars. This study assesses the performance improvement brought by the vertical and longitudinal tyre contact force signals, obtained through smart tyres, to an unscented Kalman filter (UKF) for vehicle speed and sideslip angle estimation, based on a nonlinear vehicle dynamics model. Two UKF designs, excluding and including smart tyre information, are compared by using experimental data from a purposely sensorised high-performance passenger car, along a comprehensive set of manoeuvres. The results show average $\sim$60% and $\sim$37% reductions of the root mean square values of the normalised vehicle speed and sideslip angle estimation errors for the filter design receiving the smart tyre information. In comparison with the more conventional UKF design without tyre force inputs, the smart tyre based estimator is also characterised by significantly enhanced robustness and adaptability to typical variations of vehicle and tyre parameters, such as the tyre-road friction coefficient.

ARTICLE HISTORY
Received 2 March 2021
Revised 4 July 2021
Accepted 10 August 2021

KEYWORDS
Sideslip angle estimation; vehicle speed estimation; tyre-road friction coefficient; smart tyre system

1. Introduction

The operation of modern integrated vehicle dynamics controllers is enabled by the information on vehicle states. State estimators play a crucial role in providing the information on vehicle variables that are not easily measurable, among which the most important ones are the sideslip angle, typically considered at the centre of gravity, and vehicle speed. An accurate estimation of these variables is needed throughout the variety of possible driving conditions, ranging from normal to limit driving scenarios, including quasi-steady-state and transient operation as well as concurrent longitudinal and lateral accelerations.

The literature highlights that simple estimation solutions have significant limitations in specific scenarios. For example, in terms of vehicle speed estimation, Song et al. [1] show

CONTACT Aldo Sorniotti a.sorniotti@surrey.ac.uk

that: (i) a vehicle speed estimation algorithm based on a single-wheel model is not effective whenever the wheel is braked or driven; and (ii) the integration of the measured longitudinal acceleration over time leads to significant errors in low-speed and wheel locking conditions. The estimation challenge becomes significantly more complex when sideslip angle estimation is considered. To cope with the variety of handling scenarios, many studies from the recent literature adopt state estimation algorithms based on Kalman filters incorporating vehicle dynamics models at various levels of accuracy. For example, in [2,3] a 2-degree-of-freedom (2-DOF) linear bicycle model is adopted, with lateral axle forces linearly dependent on slip angles, which poses issues when the vehicle operates outside the linear cornering response region. The same model is used by van Aalst et al. [4], who, however, add cornering stiffness adaptation, modelled as process noise, to cope with tyre nonlinearities. Similarly, in [5] Li et al. propose an adaptive algorithm based on a proportional integral controller to obtain the cornering stiffness of the bicycle model used for sideslip angle estimation in quasi-steady-state cornering, within a fusion system framework including a kinematic estimator as well. To appropriately consider the effect of the load transfers during high excitation and emergency driving scenarios, Li et al. [6] embed a double-track nonlinear model into an extended Kalman filter (EKF), which implies model linearisation at each time step. Doumiati et al. [7] simplify the 4-wheel nonlinear vehicle model by neglecting the wheel dynamics and by modelling the longitudinal forces as process noise. However, references [8–10] include the wheel dynamics and longitudinal force formulations in the internal model of the filter, for acceptable performance at the limit of handling. These studies use 7-DOF vehicle models, considering longitudinal, lateral and yaw dynamics as well as wheel dynamics, coupled with unscented Kalman filter (UKF) technology, which removes the burden associated with the linearisation phase of EKFs. UKFs have recently become widely adopted in automotive research, see [8–10], for their superior robustness with respect to sampling rates and approximation errors, achieved with similar level of computational effort with respect to the corresponding EKF implementations [11].

Although vehicle and/or tyre parameters are usually considered time-invariant, which reduces the complexity of the state estimator and its computational burden, some state-of-the-art estimators deal with parametric uncertainties by adding another parallel estimator of the main vehicle parameters, or by jointly estimating vehicle states and parameters. For instance, in Wenzel et al. [12] the estimation of the key vehicle states via a Kalman filter is improved by the parallel update of vehicle mass, yaw mass moment of inertia and longitudinal position of the centre of gravity, implemented through a second Kalman filter. The studies in [8–10,13,14] improve their estimator performance through the online update of the peak tyre-road friction coefficient and/or cornering stiffness.

Kalman filters based on dynamic vehicle models are the most common solution for vehicle state estimation; however, they still present significant limitations in coping with the variety of operating conditions of real vehicles. As a consequence, significant research effort is being devoted to the development of advanced solutions, including: (a) adaptive model-based Kalman filters, e.g. varying the filter covariances as functions of the vehicle states [6]; and (b) fusion systems, integrating different state estimators and sensors, e.g. see the combination of kinematic and vehicle model-based estimations in [5].

In this context, the introduction of tyre sensing systems, see [15,16], offers the possibility of making the tyre an active component of the estimation algorithm, by adding a direct

feedback contribution that enhances state estimation robustness with respect to the inaccuracies of the tyre force models. These solutions open promising perspectives in terms of vehicle state estimation and control system development, see [17–20]. In particular, with respect to state estimation, the pioneering study in [17] proposes an EKF based on a single-track model, under the assumption that the smart tyre system provides the total lateral axle force, which is used as sensor feedback in the measurement equation, while the longitudinal and vertical tyre forces are not considered. In absence of a vehicle prototype with smart tyres at the time of that preliminary study, the resulting estimator performance was assessed through vehicle dynamics simulations, under reasonable assumptions for the virtual emulation of the smart tyre system. A further limitation of that initial research is the fact that the currently available smart tyre systems, such as the one used in this study, cannot provide reliable and sufficiently accurate lateral tyre force information yet, which is the only smart tyre output considered in [17], while they have reached good estimation capability in terms of vertical tyre loads and longitudinal tyre forces, which, however, are not used in the filter in [17].

Similarly to smart tyres, load sensing bearing (LSB) technology can enhance vehicle state estimator performance. In the very relevant experimental study in [21], Nam et al. use the lateral forces from sensorised hubs and a recursive least square (RLS) algorithm to estimate vehicle sideslip angle. The considered single-track vehicle model is linear with constant cornering stiffness, and neglects the slip ratios as well as the interaction between longitudinal and lateral tyre forces. In [22] Nam et al. use the nonlinear version of the model in [21] in the computation of the longitudinal and lateral components of the tyre forces in the vehicle reference system, but still keep a linear tyre model, with an RLS algorithm estimating the axle cornering stiffness from the lateral forces at the wheel hubs. The lateral forces and cornering stiffness are included in the measurement vector of an EKF. The LSB based Kalman filter in [23] uses a 2-DOF linear double-track model, in which the longitudinal and lateral tyre forces are considered as inputs from the bearing systems, i.e. they are not included in the measurement equation. This formulation requires high sensor accuracy, which is improved by a specific algorithm that estimates the offsets in the LSB system. Moreover, as the LSB measurement noise cannot be modelled as a white noise, the process noise of the estimator requires an additional term, which is derived by means of simulations, in which the measurement error is studied in the time and frequency domains.

In summary, the literature shows evident research opportunities on: (i) the implementation of experimentally validated model-based estimators of vehicle speed and sideslip angle, using information from real smart tyres, rather than fictitious smart tyre signals generated by simulation models; and (ii) state estimators using measured forces, either through smart tyres or load sensing wheel hub bearings, which are based on advanced nonlinear vehicle dynamics models, i.e. incorporating longitudinal, lateral, yaw and wheel dynamics as well as tyre nonlinearities for combined cornering and braking/traction conditions.

This paper aims to cover the identified gap by further developing the activity outlined in [24]; more specifically, the novel contributions are:

- The adoption of state-of-the-art smart tyre technologies developed by Pirelli, namely the Cyber^{TM} Tyre system, for the design of a smart tyre based UKF, i.e. the so-called UKF-CT of McLaren Automotive, which includes the smart tyre signals of the longitudinal

tyre force and normal load as feedback contribution in the measurement update of the filter algorithm;
- The experimental evaluation of the estimation performance of vehicle speed, sideslip angle and peak tyre-road friction factor of the UKF-CT and its equivalent version excluding the smart tyre inputs (called UKF in the remainder), in different tyre-road friction conditions, during normal and extreme handling manoeuvres on a McLaren 570S vehicle prototype. For fairness of comparison, an optimisation routine carries out the automated calibration of the main estimator parameters;
- The sensitivity analysis of the UKF estimation performance with respect to vehicle and tyre parameter variations, with and without the inputs from the smart tyre system.

The remainder is organised as follows: Section 2 is an overview on the considered smart tyre system and vehicle prototype; Section 3 presents the state estimator architecture and the experimental validation of its internal vehicle model; Section 4 describes the adopted UKF tuning routine, and shows the comparison between the UKF–CT and UKF in terms of performance and robustness; finally, Section 5 summarises the main conclusions.

2. The case study smart tyre system and demonstrator vehicle

From a vehicle dynamics perspective, tyres are in the most privileged position as they are the only component that is in contact with the road surface. Sensing systems directly located in the tyre are a promising technology to obtain useful information for vehicle dynamics control and/or state estimation. Accordingly, the Cyber^{TM} Tyre project of Pirelli Tyre S.p.A. is developing an innovative tyre sensing system that is able to: (i) measure the relevant variables through a tri-axial accelerometer embedded in the inner liner of the tyre carcass; (ii) condition the collected signals during the tyre rolling motion; and (iii) transmit them to a receiver located on the vehicle. The outputs of the specific smart tyre system are: (a) the vertical and longitudinal tyre forces, detected once per wheel rotation, which represent the smart tyre outputs used in this study; (b) a flag variable that provides indication of incipient hydroplaning, see [25]; and (c) indication of the installed tyre model, i.e. the so-called tyre ID function, which allows automated re-tuning of the tyre parameters included in the vehicle state estimators and controllers when the tyres are replaced with a different model. The algorithms for the generation of the variables in (a)–(c), developed through indoor calibration tests in controlled environment, are beyond the scope of this paper, and are described in [26].

In the practical implementation, the smart tyre system outputs have a non-negligible time delay, consisting of three contributions: (i) a variable time delay component, which is inversely proportional to the wheel speed, and corresponds to the time needed by the smart tyre sensor to provide a meaningful measurement to the sensor processing unit; (ii) a constant elaboration time delay ($\sim$4–5 ms); and (iii) a variable time delay component dependent on the CAN bus refresh time. These delays are present in all experimental measurements discussed in the remainder.

Smart tyre systems can be used as a tool to enhance both the vehicle development process and vehicle dynamics performance. In the block diagram in Figure 1, the upper level covers the typical vehicle dynamics development steps, including the definition of the passive vehicle behaviour, and the design of vehicle dynamics control systems. The smart

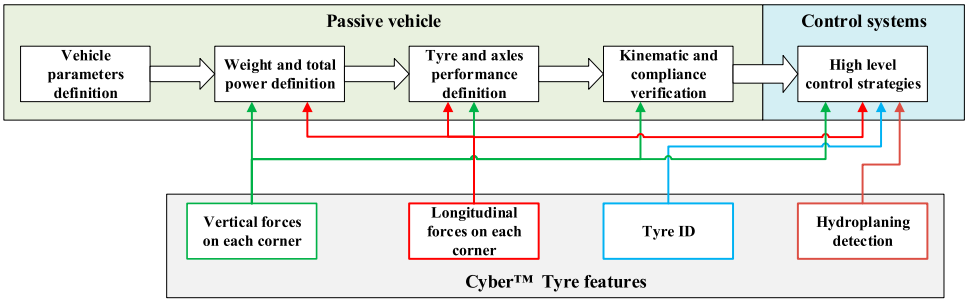

Figure 1. Enhanced vehicle development process through the Cyber^{TM} Tyre features.

Figure 2. (a) Sensorised McLaren 570S prototype; and (b) handling circuit of the IDIADA proving ground (https://www.applusidiada.com, last accessed on 1/3/2021).

tyre features are in the lower level of the diagram, and enable informed vehicle development and operation. For instance, the vertical and longitudinal tyre forces are useful inputs for suspension kinematics and compliance evaluation during real driving in the vehicle testing phase, including verification of the anti-dive/-lift/-squat and bump stop characteristics. Nonetheless, the main benefit of smart tyre systems is the enhancement of the high-level vehicle control strategies, including state estimators, agility and stability controllers, wheel slip controllers, active and semi-active suspension controllers, and individual wheel steering controllers.

The study of this paper focuses on the assessment of the vehicle speed and sideslip angle estimation benefits of the case study smart tyre system, which has been integrated with the state estimation system developed by McLaren Automotive and the University of Surrey. The analysis is based on a selection of experimental results obtained from the installation of Pirelli P Zero Corsa tyres (with different sizes on the front and rear axles), sensorised through Cyber^{TM} Tyre technology, on the rear-wheel-drive McLaren 570S prototype in Figure 2(a), which was driven along the handling circuit of the IDIADA proving ground (Spain, see Figure 2(b)). The main vehicle parameters are reported in Table 1. In addition to the smart tyre system and the conventional on-board sensors, the test vehicle was equipped with an OxTS RT unit [27] and a 6D inertial measurement unit (IMU-AB12 [28]), which provide accurate measurements of the vehicle body acceleration and speed components for state estimation validation.

Table 1. Main vehicle parameters.

Symbol	Description and unit	Value
H_{CoG}	Centre of gravity (*CoG*) height (m)	0.440
l	Wheelbase (m)	2.670
l_F	Front semi-wheelbase, i.e. distance from front axle to *CoG* (m)	1.535
$M_{ICE,max}$	Maximum engine torque (Nm @rpm)	620 @5500÷6500
m	Vehicle mass (kg)	1708
P_{max}	Maximum power (kW @rpm)	441 @7500
t_F	Front track width (m)	1.689
t_R	Rear track width (m)	1.630

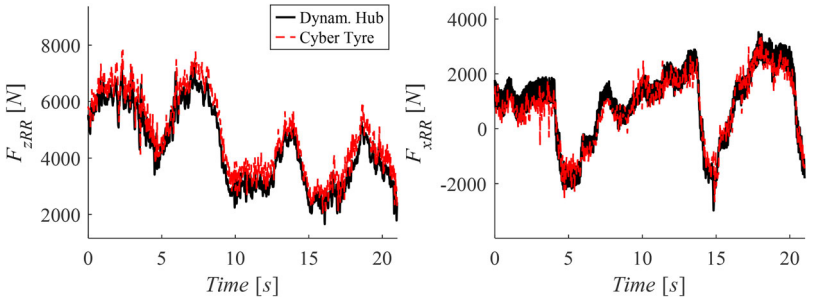

Figure 3. Comparison between the vertical and longitudinal forces on the rear right wheel, respectively F_{zRR} and F_{xRR}, measured by a dynamometric hub and generated by the Cyber^{TM} Tyre system along a portion of the handling circuit in Figure 2(b).

Figure 3 shows an example of estimation performance of the smart tyre system installed on the case study vehicle, in terms of normal and longitudinal forces, respectively F_{zRR} and F_{xRR}, on the rear right vehicle corner during an experimental test in the handling circuit in Figure 2(b), involving significant longitudinal and lateral accelerations. The comparison between the forces measured by a commercial RoadDyn dynamometric hub and the corresponding values from the Cyber^{TM} Tyre system highlights the accuracy of the latter. This is confirmed by Figure 4, in which the colour scale reports the magnitude of the force errors as functions of the longitudinal and lateral acceleration levels (the so-called 'g-g diagram') during a lap on the handling track.

3. State estimator design

This section describes the vehicle model embedded in the proposed UKF, its experimental validation, and the UKF algorithms for state and parameter estimation.

3.1. Internal vehicle model formulation

A nonlinear dynamic 7-degree-of-freedom (7-DOF) double-track model is chosen as internal vehicle model for the two UKF implementations. The model considers the longitudinal,

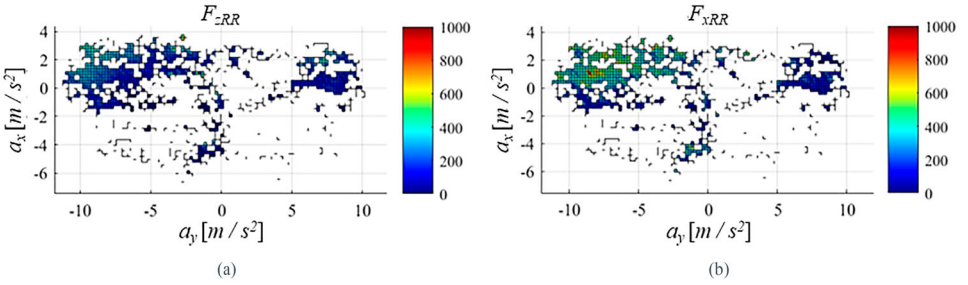

Figure 4. Absolute values (expressed in N) of the vertical (a) and longitudinal (b) force estimation errors between the Cyber™ Tyre system and a RoadDyn dynamometric hub along a portion of the handling circuit in Figure 2(b).

lateral and yaw dynamics, as well as the rotational wheel dynamics. The main assumptions are:

- The motion is planar, and thus the road bank and inclination angles are neglected, which does not represent a limitation in most conditions, given the robustness of the resulting estimator;
- The heave and pitch dynamics are disregarded;
- The rear drivetrain torques and the braking torques on each corner are known in a first approximation, and are obtained from messages that are already commonly available on the CAN (controller area network) bus of the specific vehicle. For example, the braking torque values are estimated from the tandem master cylinder pressure message.

Figure 5 shows the vehicle schematic, with positive directions of the main vectors and variables, according to the ISO convention [29]. In the following formulations, the subscript i, with $i = F, R$, indicates the axle, whereas the subscript j, with $j = L, R$, indicates the vehicle side. In the figure, V is the vehicle speed, having longitudinal and lateral components v_x and v_y; β is the sideslip angle; F_{xij} and F_{yij} are the longitudinal and lateral tyre forces; δ_{Fj} is the steering angle of the front wheels; $\dot{\psi}$ is the vehicle yaw rate; t_i is the track width; l_i is the longitudinal distance between the centre of gravity, CoG, and the axle i; and Δy_{CoG} is the lateral position of the CoG with respect to the plane of symmetry of the vehicle. In addition to the steering angles, the model inputs are represented by the engine and individual braking torque values, M_{ICE} and M_{Bij}.

The longitudinal force balance equation is:

$$a_x = \dot{v}_x - \dot{\psi} v_y = \frac{1}{m}\left\{\sum_{j=L,R}\left[F_{xFj}\cos\delta_{Fj} - F_{yFj}\sin\delta_{Fj}\right] + \sum_{j=L,R} F_{xRj} - F_{drag}\right\} \tag{1}$$

where a_x is the longitudinal acceleration; m is the vehicle mass; and F_{drag} is the aerodynamic drag force. The lateral force balance equation is:

$$a_y = \dot{v}_y + \dot{\psi} v_x = \frac{1}{m}\left\{\sum_{j=L,R}\left[F_{xFj}\sin\delta_{Fj} + F_{yFj}\cos\delta_{Fj}\right] + \sum_{j=L,R} F_{yRj}\right\} \tag{2}$$

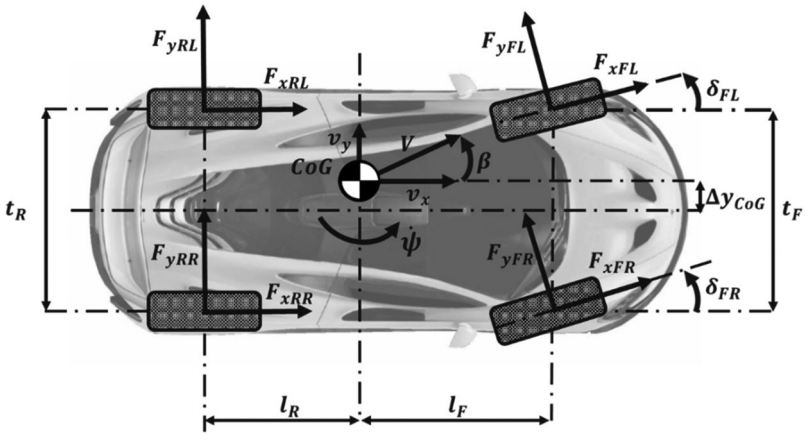

Figure 5. Top view of the vehicle with main parameters and variables.

where a_y is the lateral acceleration. The yaw moment balance equation is:

$$\ddot{\psi} = \frac{1}{J_z}\Bigg\{ l_F \sum_{j=L,R} [F_{xFj}\sin\delta_{Fj} + F_{yFj}\cos\delta_{Fj}] + \left[\frac{t_F}{2} - \Delta y_{CoG}\right][F_{yFL}\sin\delta_{FL} - F_{xFL}\cos\delta_{FL}]$$
$$- \left[\frac{t_F}{2} + \Delta y_{CoG}\right][F_{yFR}\sin\delta_{FR} - F_{xFR}\cos\delta_{FR}]$$
$$- \left[\frac{t_F}{2} - \Delta y_{CoG}\right]F_{xRL} + \left[\frac{t_R}{2} + \Delta y_{CoG}\right]F_{xRR}$$
$$- l_R \sum_{j=L,R} F_{yRj} + \sum_{i=F,R}\sum_{j=L,R} M_{zij}\Bigg\} \tag{3}$$

where J_z is the yaw mass moment of inertia, and M_{zij} is the self-aligning moment of the tyres. The vehicle speed and sideslip angle are given by:

$$V = \sqrt{v_x^2 + v_y^2} \tag{4}$$

$$\beta = \tan^{-1}\left(\frac{v_y}{v_x}\right) \tag{5}$$

In (5) and the remainder, the notation '( )' indicates the argument of a function. The dynamics of each wheel are described by a moment balance equation, which, for the rear wheels, is:

$$J_{w_{eqRj}}\dot{\omega}_{Rj} = \ 0.5M_{ICE}i_{tr}\eta_{tr} - M_{BRj} - F_{xRj}R_{lRj} - M_{yRj} \tag{6}$$

where $J_{w_{eqRj}}$ is the equivalent mass moment of inertia of the wheel, including the contribution of the powertrain components; $\dot{\omega}_{Rj}$ is the angular wheel acceleration; i_{tr} is the transmission gear ratio; and η_{tr} is the transmission efficiency.

The Pacejka Magic Formula (version 2002, see [30]) calculates the rolling radius, laden radius, rolling resistance, longitudinal force, lateral force, and aligning moment of the tyres,

namely R_{eij}, R_{lij}, M_{yij}, F_{xij}, F_{yij}, and M_{zij}, as functions of the tyre slip angle α_{ij}, longitudinal slip ratio σ_{xij}, vertical load F_{zij}, and camber angle γ_{ij}, which is expressed as a function of the longitudinal load transfer and roll angle ϕ, given by the following approximated static formulation:

$$\phi = \frac{m[H_{CoG} - H_{RA,CoG}]}{K_{\phi F} + K_{\phi R}}[a_y \cos\phi + mg \sin\phi] \tag{7}$$

where $K_{\phi i}$ is the roll stiffness of the considered axle; H_{CoG} is the centre of gravity height; and $H_{RA,CoG}$ is the roll axis height at the longitudinal coordinate of the centre of gravity. To ensure stable operation of the tyre model also in low-speed conditions, the conventional formulations of the longitudinal and lateral slips, σ_{xij} and α_{ij}, are modified according to the stability analysis in [31,32]:

$$\sigma_{xij} = \frac{\omega_{ij} R_{eij} - v_{xij}}{\max(|v_{xij}|, \eta_{lng} v_{x,lng,marg})} \tag{8}$$

$$\alpha_{ij} = \tan^{-1}\left(\frac{V \sin\beta \pm \dot{\psi} l_F}{\max\left(\eta_{lat} v_{x,lat,marg}, \left|V \cos\beta \mp \frac{\dot{\psi} t_F}{2}\right|\right)}\right) - \delta_{Fj} \tag{9}$$

where v_{xij} is the longitudinal component of the peripheral wheel speed; ω_{ij} is the angular wheel speed; $v_{x,lng,marg}$ and $v_{x,lat,marg}$ are the marginal speeds, namely the minimum speed values preventing longitudinal and lateral slip singularities; and η_{lng} and η_{lat} are positive safety coefficients. This formulation facilitates the removal of tyre slip and force oscillations, which can lead to numerical instability and may affect the state estimator performance. This phenomenon is more evident with high time steps of the numerical integration process; the authors of [31,32] define the minimum marginal speed as a function of the simulation time step. Moreover, as the marginal speed depends on the longitudinal slip stiffness and cornering stiffness of the considered tyres, in this study, differently from [31,32], it has been varied according to the stiffness values resulting from the Magic Formula. As this study is focused on the sideslip angle estimation enhancement associated with smart tyre systems, tyre relaxation was not considered essential for the implementation of the filters, given the already satisfactory results, also in consideration of the trade-off between computational efficiency and filter performance. However, the inclusion of tyre relaxation could be a relevant future development, especially to enhance the estimation performance during events characterised by significantly high dynamics at the wheel level, e.g. during the intervention of the anti-lock braking or traction control systems.

The computation of the vertical tyre loads on each corner, F_{zij}, includes consideration of the longitudinal and lateral load transfers and aerodynamic downforce contributions:

$$\begin{aligned} F_{zFj} &= \frac{0.5 t_F \mp \Delta y_{CoG}}{t_F}\left[\frac{l_R mg}{l_F + l_R} + \frac{F_{df\%}}{100} F_{df,F}\right] - \Delta F_z^x \mp \Delta F_{zF}^y \\ F_{zRj} &= \frac{0.5 t_R \mp \Delta y_{CoG}}{t_R}\left\{\frac{l_F mg}{l_F + l_R} + \left[1 - \frac{F_{df\%}}{100}\right] F_{df}\right\} + \Delta F_z^x \mp \Delta F_{zR}^y \end{aligned} \tag{10}$$

where g is the gravitational acceleration; F_{df} is the total aerodynamic downforce; and $F_{df\%}$ is the front-to-total aerodynamic downforce distribution. The longitudinal load transfer

caused by acceleration and braking, ΔF_z^x, is given by:

$$\Delta F_z^x = \frac{1}{2}\frac{H_{CoG} m a_x}{l_F + l_R} \tag{11}$$

The front and rear lateral load transfers, ΔF_{zF}^y and ΔF_{zR}^y, are evaluated through steady-state equations, considering the lateral acceleration and anti-roll moment distribution between the front and rear axles:

$$\begin{aligned}
\Delta F_{zF}^y &= \frac{a_y}{t_F}\left\{ m\frac{l_R}{l} H_{RC,F} + \frac{M_{\phi\%}}{100}\left[mH_{CoG} - m\frac{l_R}{l} H_{RC,F} - m\frac{l_F}{l} H_{RC,R} \right] \right\} \\
\Delta F_{zR}^y &= \frac{a_y}{t_R}\left\{ m\frac{l_F}{l} H_{RC,R} + \left[1 - \frac{M_{\phi\%}}{100} \right]\left[mH_{CoG} - m\frac{l_R}{l} H_{RC,F} - m\frac{l_F}{l} H_{RC,R} \right] \right\}
\end{aligned} \tag{12}$$

where $M_{\phi\%}$ is the front-to-total anti-roll moment distribution; and $H_{RC,F}$ and $H_{RC,R}$ are the roll centre heights of the front and rear suspensions.

3.2. Experimental validation of the internal vehicle model

The experimental validation of the internal model was achieved by comparing the model outputs with measured data from the case study vehicle, along a set of manoeuvres covering a wide range of longitudinal and lateral accelerations, in steady-state and transient conditions. As suggested in [33], the selected manoeuvres are: (i) swift acceleration up to 9 m/s^2 followed by hard braking up to ~ -15 m/s^2 in straight line, with the vehicle reaching a top speed of 110 km/h. This manoeuvre is abbreviated as SA+HB. The significant acceleration values are made possible by the high-performance characteristics of the case study vehicle; (ii) slow ramp steer (SRS) at the approximately constant speed of 150 km/h, with a steering wheel rate of 20 deg/s and a maximum steering wheel angle magnitude of 140 deg (iii) sine chirp (SC) steering test at 150 km/h, with a steering wheel angle amplitude of 20 deg applied at a maximum frequency of 0.6 Hz; and (iv) step steer (SS) test from an initial speed of 100 km/h, with a final steering wheel angle of 100 deg.

In the validation, the model input variables are δ_{Fj}, M_{ICE} and M_{Bij}; the model output variables are a_x, a_y, $\dot{\psi}$ and V for all manoeuvres, whereas β and ϕ are evaluated only during the lateral dynamics tests, i.e. tests (ii)–(iv), due to the low reliability of the corresponding measurements during straight line manoeuvres. Figure 6 summarises the model validation results through bisector diagrams comparing the measurements and model outputs, in terms of sideslip angle, yaw rate, lateral acceleration, roll angle, vehicle speed, and longitudinal acceleration. The target, indicated as 'Tgt' in the figure, is to keep the points of the plots as close as possible to the quadrant bisector, which is the ideal condition in which the model outputs perfectly match the measurements. The marginal overestimation of most of the variables is related to the inevitable simplifications in the tyre model and suspension elasto-kinematic behaviour within the internal model of the filter, in the context of a trade-off between model fidelity and computational requirements. The model simplifications tend to increase the level of cornering response of the simulated vehicle with respect to the real one for given vehicle speed and steering input. The underestimation of the longitudinal deceleration during hard braking conditions is caused by the fact that in the specific test the anti-lock braking system (ABS) was activated on the real vehicle. The

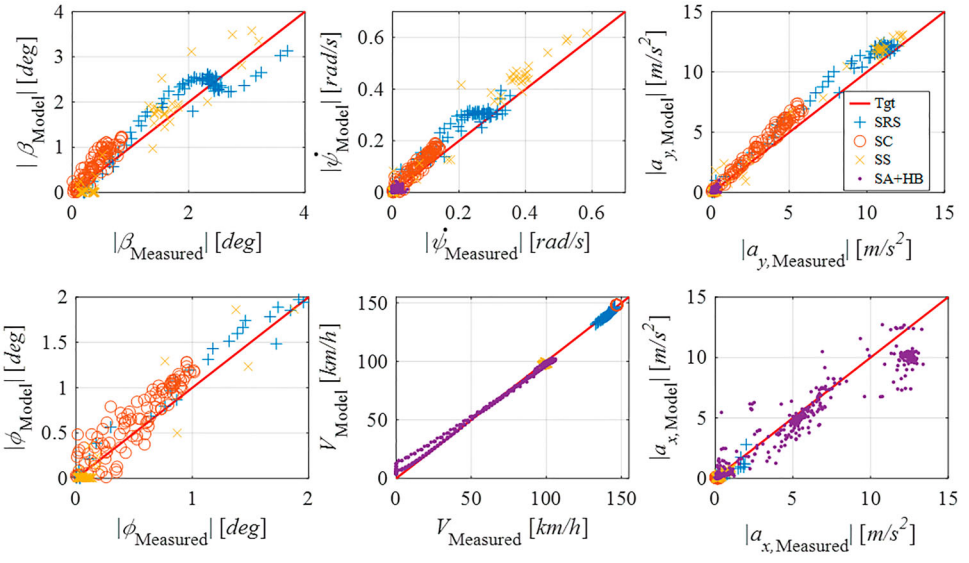

Figure 6. Bisector diagrams for plant model validation.

internal model of the filter running in open loop is not equipped with the ABS, and therefore – to prevent wheel locking during the model validation phase, and in absence of the knowledge of the individual wheel caliper pressure profile during the ABS activation on the real vehicle – the tandem master cylinder pressure used in the model had to be kept at a marginally lower level than in the experiments in the hard braking phases, which generated a lower deceleration value. Despite the minor performance differences between the model and the real plant, based on the extensive set of tests the internal model of the filters can be considered a reliable tool for predicting the response of the real vehicle.

3.3. Parameter estimation

Model based state estimates are strongly dependent on the varying vehicle parameters, e.g. mass and centre of gravity position, and tyre parameters, including the tyre-road friction coefficient μ. In particular, tyre parameter accuracy is fundamental in determining the contact forces. In [34], parameter estimation is accomplished by extending the plant model in the time update of the filter with an additional state-space equation with a new variable, i.e. the estimated parameter, which is described by a random walk model (RWM), a stationary process only driven by the corresponding process noise.

In this study, similarly to [17], the estimated parameter is the peak tyre-road friction factor, μ_{max}, which is integrated in the Pacejka Magic Formula 2002 as a scaling parameter of D_{xij} and D_{yij}, namely the peak factors on the wheel ij in pure longitudinal and lateral slip conditions, which are expressed as in [30]:

$$\begin{aligned} D_{xij} &= F_{zij}[p_{Dx1} + p_{Dx2}df_{zij}][1 - p_{Dx3}\gamma_{xij}^2]\lambda_{\mu x}\mu_{max} \\ D_{yij} &= F_{zij}[p_{Dy1} + p_{Dy2}df_{zij}][1 - p_{Dy3}\gamma_{yij}^2]\lambda_{\mu y}\mu_{max} \end{aligned} \tag{13}$$

where df_{zij} is the normalised vertical load of the wheel ij; p_{Dxn} and p_{Dyn}, with $n = 1,\dots,3$, are the shape factors in pure slip conditions; the terms γ_{xij} and γ_{yij} are linear functions of the camber angle of the respective wheel; $\lambda_{\mu x}$ and $\lambda_{\mu y}$ are the scale factors of the friction coefficient in pure longitudinal and lateral slip conditions, set to 0.94. The dynamics of the peak tyre-road friction factor are described by $\dot{\mu}_{max} = 0$, which, in discretised form, becomes:

$$\mu_{max,k} = \mu_{max,k-1} + w_{\mu_{max},k-1} \tag{14}$$

where k is the discretisation step, and $w_{\mu_{max},k-1}$ is the associated process noise. In the proposed filters, the purpose of the μ_{max} estimation is to enhance the estimation of the main filter outputs, e.g. vehicle speed, sideslip angle, and lateral tyre forces, rather than achieving an accurate friction estimation. In this respect, μ_{max} constitutes an additional degree of freedom, which increases the vehicle model robustness by scaling the tyre-road friction coefficient in the Pacejka tyre model formulation [8,9,14].

3.4. Unscented Kalman filter implementation

UKFs ([34]) are based on an iterative process that consists of two main steps: (i) a time update, in which the set of nonlinear equations describing the n states of the plant model are subject to forward Euler explicit integration to compute the *a-priori* state vector, x^-; and (ii) a measurement update, in which the error between the predicted measurement and real data, i.e. e_y^-, is fed back to correct the estimation based on the internal model equations [35].

Within the UKF algorithm, the nonlinear model used in step (i) is arranged as:

$$\begin{cases} x_k = f(x_{k-1}, u_k, w_{k-1}) \\ y_k = h(x_k, u_k, v_k) \end{cases} \tag{15}$$

where f describes the system dynamics; h is the observation model; $x_k \in \mathbb{R}^n$ is the state vector at the time step k, assumed to have Gaussian probability distribution $P_k \in \mathbb{R}^n$; $u_k \in \mathbb{R}^r$ and $y_k \in \mathbb{R}^m$ are the input and output vectors; and the random variables $w_{k-1} \in \mathbb{R}^n$ and $v_k \in \mathbb{R}^m$ are the process and measurement noise vectors. The noise vectors are assumed to be white and uncorrelated with zero-mean Gaussian probability distributions defined by the covariance matrices $Q \in \mathbb{R}^{n\times n}$ and $R \in \mathbb{R}^{m\times m}$. As the noise components are uncorrelated, the covariance matrices are diagonal. Ideally, Q and R should change at each iteration because the uncertainties related to the process and sensors might vary. However, unlike P_k, Q and R are kept constant to reduce the computational load, and aid the estimation of the error covariance P_k and the Kalman gain K_k to quickly converge and stabilise [35]. To avoid neglecting any odd-moment information, in the computation of K_k the UKF algorithm uses an augmented state vector, x_{aug}, with size $N = 2n + m$, and the corresponding augmented error system covariance matrix, P_{aug}, see [8,11]:

$$x_{aug} = \{x_{k-1} \quad w_{k-1} \quad v_k\}^T; \quad P_{aug} = \begin{bmatrix} P_{k-1} & 0 & 0 \\ 0 & Q & 0 \\ 0 & 0 & R \end{bmatrix} \tag{16}$$

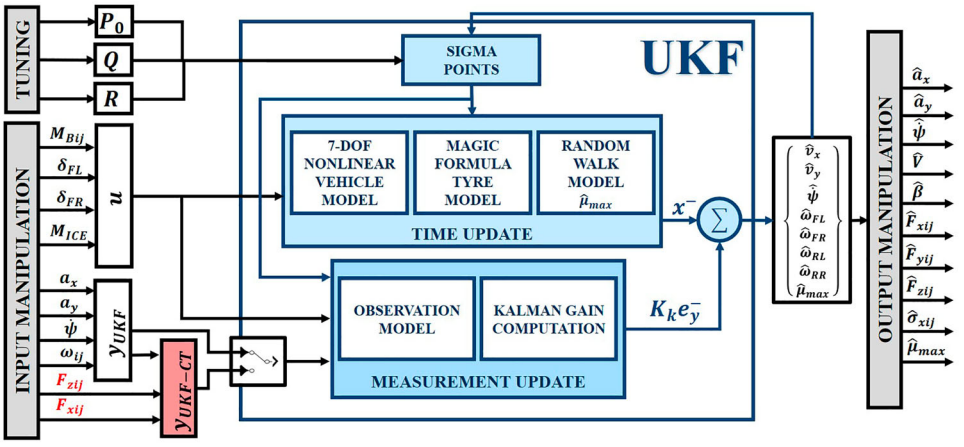

Figure 7. Schematic of the UKF algorithm for vehicle state estimation.

The measurement update in step (ii) is described by:

$$x_k^+ = x_k^- + K_k e_{y,k}^- = x_k^- + K_k[y_k - y_{UKF/UKF-CT}] \tag{17}$$

where x_k^+ is the *a-posteriori* estimate, i.e. the final output from the filter; x_k^- is the *a-priori* estimate, i.e. the output from the internal model; and K_k is calculated according to the steps described in [36], here omitted given the vehicle focus of this paper. Figure 7 shows the schematic of the UKF-CT implementation, whose main goal is to obtain the values of β and V, on top of other relevant variables, such as the individual lateral tyre forces, slip angles, and slip ratios. The state and input vectors resemble the experimentally validated design adopted by Antonov et al. [8]. The output vector includes variables commonly available on the controller area network (CAN) of the vehicle. Moreover, due to the availability of the estimated F_{xij} and F_{zij} from the smart tyre system, the vector y is augmented accordingly. Hence, the resulting vectors are:

$$\begin{aligned} x &= \{v_x \quad v_y \quad \dot{\psi} \quad \omega_{ij} \quad \mu_{\max}\} \\ u &= \{\delta_{Fj} \quad M_{ICE} \quad M_{Bij}\} \\ y_{UKF} &= \{a_x \quad a_y \quad \dot{\psi} \quad \omega_{ij}\} \\ y_{UKF-CT} &= \{y_{UKF} \quad F_{zij} \quad F_{xij}\} \end{aligned} \tag{18}$$

where the subscripts UKF and UKF-CT, used here and in the remainder, refer to the estimators excluding and including the smart tyre system estimates. The angular wheel speeds allow an accurate estimation of vehicle speed in most driving scenarios; the additional measurement of a_x, not included the implementation in [8], helps preventing performance degradation in conditions of significant longitudinal tyre slip.

In the filter implementation phase, the measurement noise covariance R, i.e. the variance of the sensors, was determined through the a-priori analysis of sample measurements [35], whilst the matrix Q, which considers model uncertainties, was obtained through the optimisation routine in Section 4. To reduce the number of tuning parameters, the initial error

system covariance matrix, $P_k|_{k=0}$, is set to be equal to the process noise covariance matrix, i.e. $P_k|_{k=0} = Q$, as in [10]. The additional parameters are α_{UT}, a constant defining the spread of the sigma points, which is set to 1 in the proposed implementations; β_{UT}, a constant related to the type of probability distribution, equal to 2 for Gaussian distribution; and κ_{UT}, a scaling parameter, set to $3 - N$, as recommended by [8,34,36].

3.5. Ancillary algorithms for updating mass and mass distribution

Outside the UKF-CT, an algorithm using the tyre load measurements from the smart tyre system readjusts the total vehicle mass and mass distribution for the filter and the other vehicle controllers, when pre-defined conditions are satisfied for a certain amount of time. For instance, whenever the car travels along an approximately straight line at constant speed, the vertical load signals on each corner, F_{zij}, are averaged along time. Once the system has considered a total number of samples, $N_{s,update}$, corresponding to the desired time interval $T_{update} = N_{s,update} t_s$ (T_{update} =5 s in the specific implementation of this paper, where t_s is the sampling time of the data acquisitions) in the selected driving condition, the updated average mass for the corner ij is given to the UKF-CT and the vehicle controllers, according to:

$$m_{ij,new} = \frac{1}{N_{s,update}} \sum_{p=1}^{N_{s,update}} \frac{F_{zij,p}}{g} \tag{19}$$

Hence, the total mass of the car, m, as well as the longitudinal and lateral positions of the centre of gravity, defined by l_R and Δy_{CoG}, are periodically updated according to the following formulations:

$$\begin{aligned} m_{new} &= \sum_{i=F,R} \sum_{j=L,R} m_{ij} \\ l_{R,new} &= \frac{m_{RL,new} + m_{RR,new}}{m_{new}} l \\ \Delta y_{CoG,new} &= \left[\frac{m_{FL,new} + m_{RL,new}}{m_{new}} - \frac{1}{2} \right] t \end{aligned} \tag{20}$$

where the subscript '*new*' indicates the updated parameters, and t is the average track width.

4. Results and discussion

Although the unscented Kalman filter algorithm implies the processing overhead of computing multiple sigma points at each iteration, the state estimators in Section 3 were implemented in real-time on the dSpace MicroAutobox II DS1401 rapid control prototyping unit installed on the demonstrator vehicle in Figure 2(a), with a time step of 20 ms. The signals used for the operation of the filters are already available on the CAN bus of the baseline configuration of the vehicle, whilst the additional measurements from the OxTS RT unit and 6D IMU are employed to evaluate the estimation performance. The involved car maker is currently assessing the implementation of the considered estimators also on available automotive control hardware for production vehicles.

4.1. Optimisation based tuning routine

During the study it was empirically verified that the proposed filters are stable for a wide range of settings of Q, and that reasonable nominal settings obtained through brute force trial-and-error tuning can provide good performance, which is rather close to the optimal one. However, in the specific activity, to present the capability of the filters at their best and for fairness of comparison, an optimisation routine was implemented to find the optimal values of the elements on the diagonal of the covariance matrix Q of the UKF and UKF-CT, along a comprehensive set of experimental training manoeuvres. Due to the complexity and significant nonlinearities, a multi-objective genetic algorithm was selected, using six objective functions, based on the normalised root mean square error (*NRMSE*) between: (i) the experimental data from the OxTS RT unit, the 6D IMU, and the Cyber^{TM} Tyre system, here used as a development tool for both the UKF and UKF-CT; and (ii) the estimation outputs, obtained by feeding the filters with the required CAN bus signals during the same training manoeuvres. The optimisation problem is defined by:

$$\begin{aligned} &\min_{\arg Q} \; J_b \quad \text{s.t.} \quad Q_h \in [Q_{h,min}, Q_{h,max}] \\ &J_b = NRMSE(b) = \sqrt{\frac{1}{N_s}\sum_{p=1}^{N_s}\left[\frac{e_{w,b,p}}{b_{norm}}\right]^2} \quad \text{with } b = \beta, a_x, F_{xRL}, F_{xRR}, F_{zFL}, F_{zRR} \end{aligned} \tag{21}$$

where the notation J_b indicates the objective functions, accounting for the estimation accuracy of sideslip angle, longitudinal acceleration, longitudinal forces on the rear driving axle, and vertical tyre loads on opposite vehicle corners, as indicated by the index b; N_s is the number of samples in the considered time history; $e_{w,b,p}$ is the weighted estimation error of the sample p; and $Q_{h,min}$ and $Q_{h,max}$ define the range of variation of each element, Q_h, of Q. Depending on the objective function, the normalisation values, b_{norm}, are 20 deg for the sideslip angle, 12 m/s^2 for the longitudinal acceleration, 6800 N for the longitudinal tyre force on the driving axle, and 3800 N and 4750 N for the vertical tyre loads on the front and rear axles. $e_{w,b,p}$ is defined as:

$$e_{w,b,p} = \begin{cases} \hat{b}_p - b_p & \text{if } |\hat{b}_p - b_p| < e_{thr1} \\ W_1[\hat{b}_p - b_p] & \text{if } e_{thr1} \le |\hat{b}_p - b_p| < e_{thr2} \\ W_2[\hat{b}_p - b_p] & \text{if } |\hat{b}_p - b_p| \ge e_{thr2} \end{cases} \tag{22}$$

where b_p is the measured value of the considered variable; $\hat{b}_p$ is the estimated value; e_{thr1} and e_{thr2} are predefined $|\hat{b}_p - b_p|$ thresholds; and the scaling factors W_1 and W_2, with $W_2 \gg W_1 > 1$, amplify the error to penalise excessive $|\hat{b}_p - b_p|$ values in the computation of J_b. The variety of cost functions in (21) allows to obtain a filter tuning that is useful also for estimating vertical and tangential tyre forces, e.g. for effective individual wheel slip control and vehicle stability control. In the optimisation, the state vector is initialised as:

$$x_0 = \left\{0.98V_{CAN} \;\; 0 \;\; 0 \;\; 0.98\omega_{FL,CAN} \;\; 0.98\omega_{FR,CAN} \;\; 0.98\omega_{RL,CAN} \;\; 0.98\omega_{RR,CAN} \;\; \mu_{max,0,rnd}\right\} \tag{23}$$

where the initial vehicle speed and angular wheel speeds are set to 98% of their values acquired on the vehicle CAN bus, to ensure that the filter is capable of converging to the

respective actual values. β and $\dot{\psi}$ are set to 0, as the vehicle trajectories are usually straight in the initial section of the training manoeuvres. An initial random peak tyre-road friction factor value, i.e. $\mu_{max,0,rnd} \in [0.6–1.1]$, is selected for each iteration; thus, the optimisation tends to improve the convergence features of the estimator from multiple initial friction conditions.

The values of the six functions in (21) allow to build a multi-dimensional Pareto frontier. The selected optimum refers to the set of covariances identifying the closest point of the Pareto frontier to the origin of the coordinate system. The optimal covariances computed for the selected driving scenarios were used for the results in the following sections.

4.2. Experimental state estimation results and filter comparison in nominal conditions

The experimental comparison of the UKF and UKF-CT covers the following manoeuvres: (i) a slow ramp steer (SRS) at ~ 100 km/h, corresponding to quasi-steady-state cornering conditions. The steering wheel input is applied at a rate of ~ 25 deg/s, and is stopped when the steering wheel angle reaches ~ 200 deg, after which it is kept constant. Finally, at the end of the manoeuvre, the steering input is abruptly reduced; (ii) a series of lane changes in high speed conditions (HSLC), i.e. executed between 140 and 175 km/h; (iii) an open-loop step steer (SS), see ISO 7401 [37], with a steering wheel angle amplitude of 100 deg, from an initial speed of 100 km/h, followed by a final abrupt counter-steering action reaching a final steering wheel angle value of -100 deg (iv) a combined longitudinal and lateral dynamics manoeuvre with power-on (maximum longitudinal acceleration of 6 m/s^2) and final hard braking (maximum deceleration of 8 m/s^2) during a turn, with a maximum lateral acceleration of 8 m/s^2 (CPO); (v) a handling circuit lap (Figure 2(b)) on dry tarmac (DryH); and (vi) a handling circuit lap in wet tarmac conditions (WetH). For tests (i)–(v), the actual value of μ_{max} on the specific proving ground can be considered ~ 1, while for test (vi) the real μ_{max} ranges from 0.4 to 0.7. To verify their robustness, in all tests the filters were run with both initial conditions $\mu_{max,0} = 1$ and $\mu_{max,0} = 0.7$, which were imposed at the beginning of the relevant section of the manoeuvre.

Figure 8 summarises the results for the UKF and UKF-CT for $\mu_{max,0} = 1$. For both filters the samples tend to be located in proximity of the bisectors, indicated as 'Tgt', with a generally visible improvement for the UKF-CT, especially in terms of sideslip angle estimation, while vehicle speed estimation appears very good in both cases.

Key performance indicators (KPIs) are introduced to objectively assess the vehicle speed and sideslip angle estimation performance, namely:

- The root mean square value of the estimation error (expressed in percentage), normalised with respect to the maximum value of the variable (b_{max} in (24), see also the values in Table 2) along the considered set of manoeuvres, which highlights the overall estimation performance:

$$NRMSE_{\%} = 100 \sqrt{\frac{1}{N_s} \sum_{p=1}^{N_s} \left[\frac{\hat{b}_p - b_p}{b_{max}} \right]^2} \tag{24}$$

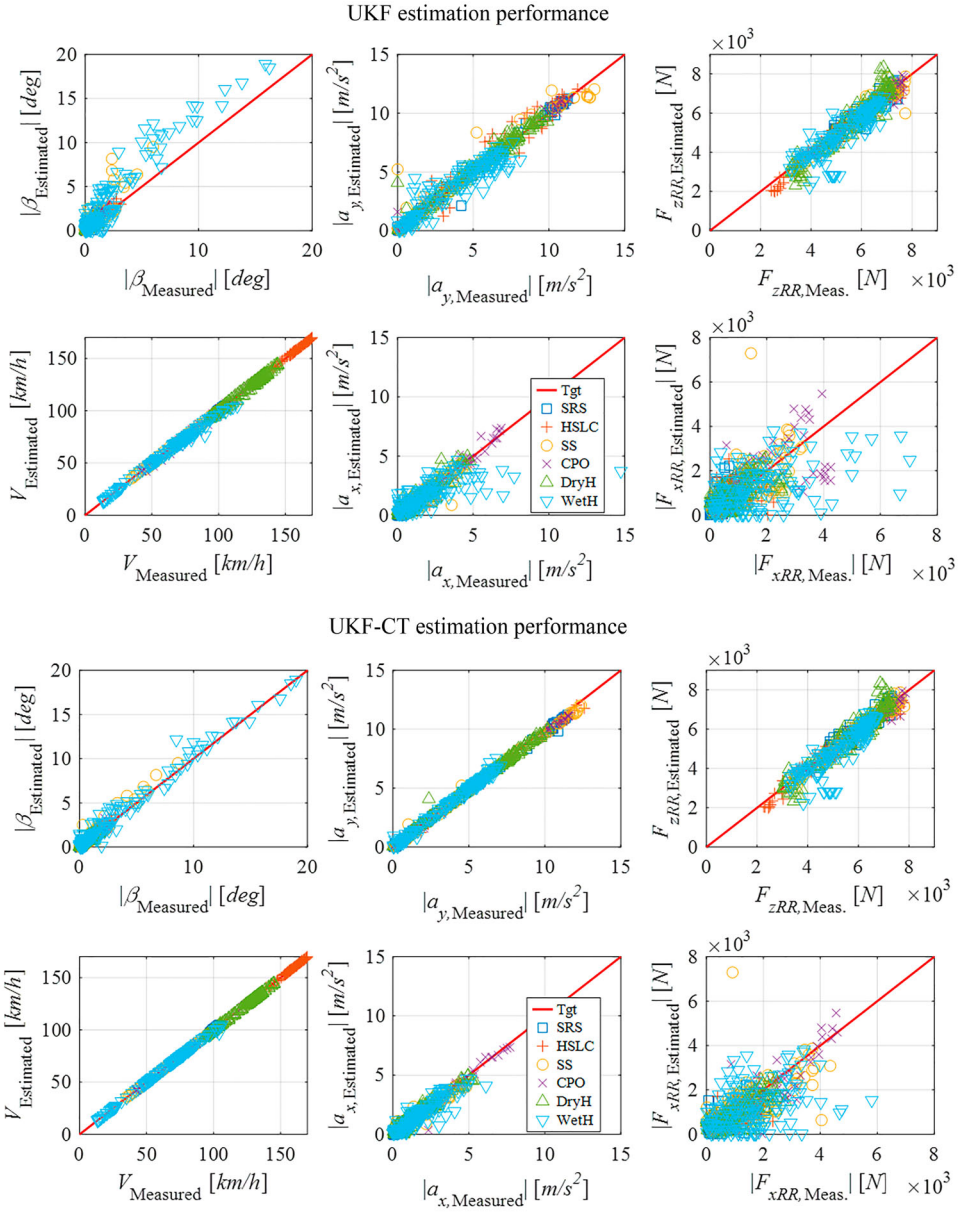

Figure 8. Bisector diagrams for the evaluation of the overall estimation performance of the UKF and UKF-CT along the considered manoeuvres, for $\mu_{max,0} = 1$.

- The normalised maximum absolute value of the estimation error, e^{max}, which evaluates the worst-case estimation performance:

$$e^{max} = 100\frac{\max|\hat{b}_p - b_p|}{|b_{max}|} \tag{25}$$

- The normalised standard deviation of the error, σ^{std}, which assesses whether the dispersion of the estimated data is limited to a certain time window or it extends along the whole manoeuvre:

$$\sigma^{std} = 100 \sqrt{\frac{1}{N_s} \sum_{p=1}^{N_s} \left[\frac{e_{b,p} - \bar{e}_{b,p}}{b_{max}} \right]^2} \tag{26}$$

where $e_{b,p} = \hat{b}_p - b_p$ and $\bar{e}_{b,p}$ are the error (without any weighting) and its mean value.

Figure 9 reports the $NRMSE_{\%}$ values of V and β, for both initial conditions of the peak tyre-road friction factor. The benefit of the UKF-CT is evident in 22 cases out of 24, as it brings an average reduction of the $NRMSE_{\%}$ of V by 46% and 73%, and an average decrease of the $NRMSE_{\%}$ of β by 49% and 26%, respectively for $\mu_{max,0} = 1$ and $\mu_{max,0} = 0.7$, in comparison with the UKF. Particularly significant are the sideslip angle estimation improvements for the slow ramp steer and step steer tests, in which the $NRMSE_{\%}$ is more than halved by the UKF-CT for both friction initialisation values. The UKF-CT addresses the weaknesses of the UKF, for which the $NRMSE_{\%}$ of β reaches the critical value of 42.7% in the slow ramp steer test from the incorrect initial friction factor. In fact, in quasi-steady-state conditions, the filter without the smart tyre system struggles converging to the actual tyre-road friction condition. Table 2 includes the e^{max} and σ^{std} values for all cases, and generally confirms the analysis of Figure 9, with 39% and 59% reductions of the maximum estimation error on vehicle speed, and 33% and 12% reductions of the maximum error on sideslip angle, brought on average by the UKF-CT with respect to the UKF, for the two initialisation values of the tyre-road friction condition. The major decrease – in excess of 30% in all cases – in the standard deviation values of the estimation errors of the UKF-CT shows the significantly more consistent performance of the smart tyre based estimator.

Figures 10–12 highlight the UKF-CT benefits in the most critical test cases. Figure 10 refers to the slow ramp steer with $\mu_{max,0} = 0.7$, while the real peak friction factor on the specific dry tarmac is ~ 1, i.e. the aim of the test is to assess the filter behaviour in quasi-steady-state conditions, with incorrect initialisation of the friction parameter. The speed estimation is comparable for the two filters, with the exception of the time window between 9 s and 11 s, when the vehicle operates at the limit of handling. This difference relates to the fast convergence of the UKF-CT to the actual value of μ_{max}, without oscillations. On the contrary, as discussed for Table 2, the random walk model of the UKF is slower in initiating the appropriate significant increase of $\hat{\mu}_{max}$. This delay brings a major overshoot in the $|\beta|$ estimation, which is followed by a sideslip angle magnitude underestimation when the RWM of the UKF overestimates the friction factor, see the time window between 10 s and 13 s, before finally approaching the correct friction value.

In the UKF tuning, optimised through the genetic algorithm, as the tyre force feedback is missing, the RWM is more aggressive, i.e. it has significantly higher covariance related to μ_{max} than in the optimal tuning of the UKF-CT. Nevertheless, this rather reactive tuning of the UKF is not sufficient to achieve good performance in the specific conditions, as mentioned by the literature. In fact, according to Grip et al. [38], during long steady-state

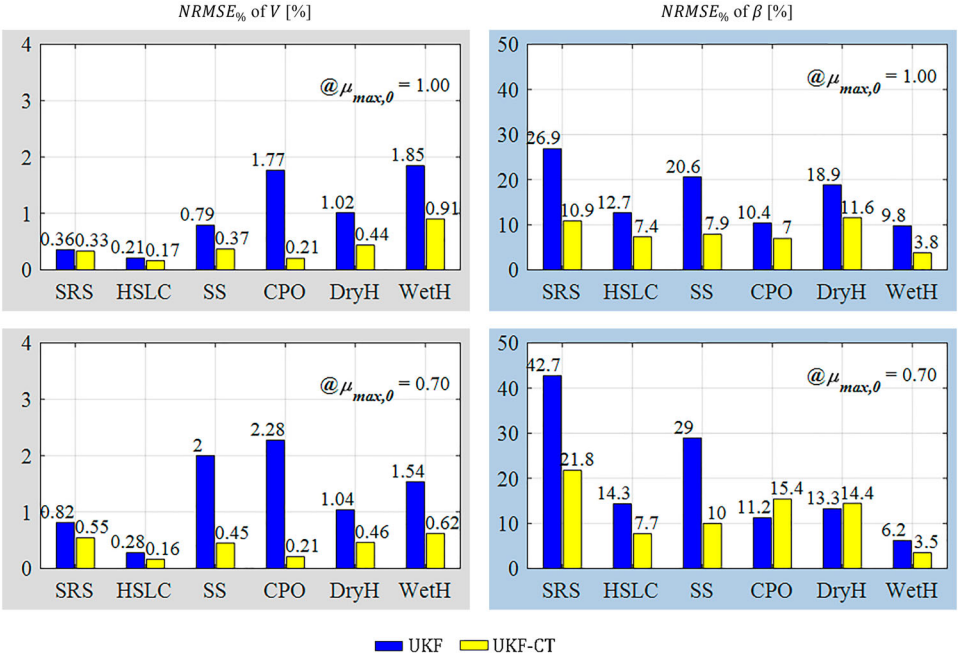

Figure 9. Performance comparison between UKF and UKF-CT in terms of $NRMSE_{\%}$ values of V and β.

Table 2. KPI values for the UKF and UKF-CT, and maximum absolute values of vehicle speed and sideslip angle along the six manoeuvres.

State	$\mu_{max,0}$	e^{max}_{UKF} [%]	e^{max}_{UKF-CT} [%]	σ^{std}_{UKF} [%]	σ^{std}_{UKF-CT} [%]	State	e^{max}_{UKF} [%]	e^{max}_{UKF-CT} [%]	σ^{std}_{UKF} [%]	σ^{std}_{UKF-CT} [%]
		Slow ramp steer					High speed lane change			
V	1.00	0.70	0.72	0.27	0.19	V	0.69	0.46	0.21	0.12
V_{max} = 105 km/h	0.70	2.58	1.16	0.80	0.23	V_{max} = 170 km/h	0.75	0.46	0.26	0.12
β	1.00	53.47	24.80	15.51	5.87	β	30.25	20.48	12.48	7.11
$\lvert\beta_{max}\rvert$ =2.4°	0.70	126.27	47.45	42.47	19.65	$\lvert\beta_{max}\rvert$ =4.0°	47.22	28.13	13.93	7.37
		Step steer					Combined power-on			
V	1.00	1.97	0.77	0.35	0.18	V	4.06	0.55	1.77	0.15
V_{max} = 103 km/h	0.70	5.05	1.25	1.97	0.30	V_{max} = 127 km/h	4.13	0.56	2.19	0.19
β	1.00	62.94	21.68	14.62	5.38	β	38.75	32.08	8.93	6.98
$\lvert\beta_{max}\rvert$ =10.0°	0.70	64.54	21.38	28.93	9.20	$\lvert\beta_{max}\rvert$ =3.5°	36.12	50.08	11.24	13.36
		Dry handling circuit					Wet handling circuit			
V	1.00	2.95	1.23	0.91	0.22	V	9.68	9.97	1.59	0.72
V_{max} = 140 km/h	0.70	3.04	1.24	0.97	0.24	V_{max} = 105 km/h	6.53	3.92	1.39	0.39
β	1.00	47.88	38.98	17.38	11.32	β	34.12	24.17	9.09	3.72
$\lvert\beta_{max}\rvert$ =1.8°	0.70	43.67	64.59	13.14	14.26	$\lvert\beta_{max}\rvert$ =20.0°	22.51	24.16	5.93	3.45

manoeuvres friction estimation via RWM is difficult to achieve because of the lack of excitation, and the suggestion is to automatically force $\hat{\mu}_{max}$ to an appropriate value during these scenarios. However, the important novel conclusion of the analysis of Figure 10 is that the vertical load and tyre force contributions from the smart tyre system are sufficient to prevent the typical tyre-road friction estimation issues and the subsequent sideslip angle estimation inaccuracies of estimators based on vehicle dynamics models, without requiring any form of additional complex rule based algorithm or adaptation mechanism.

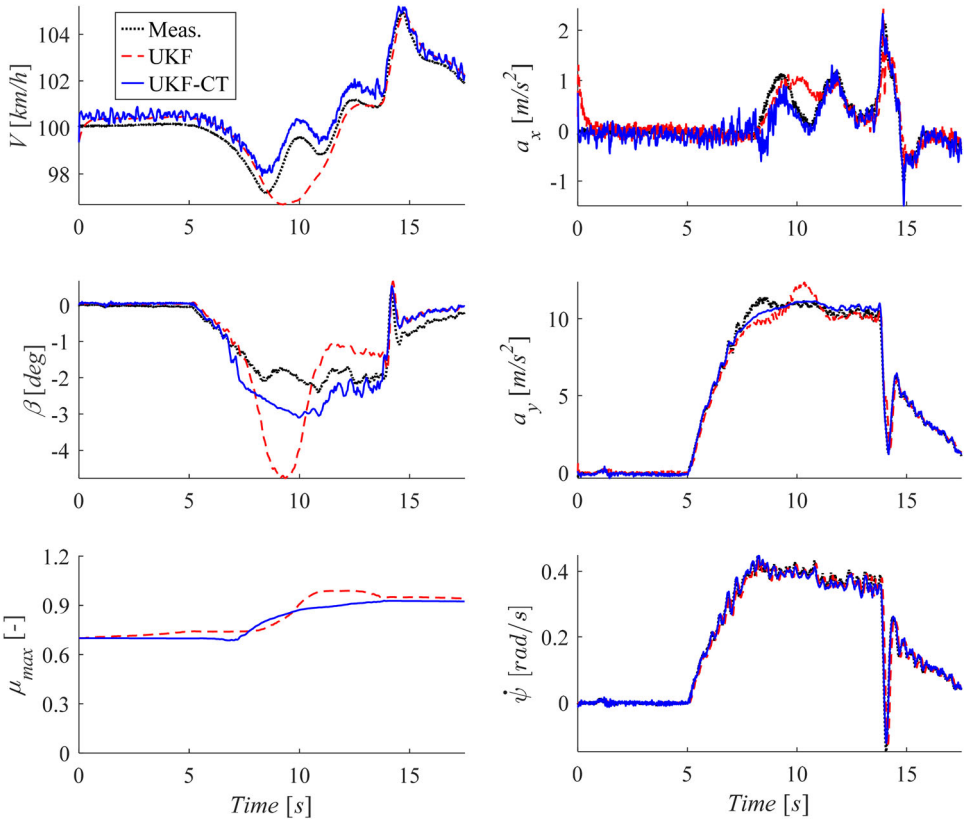

Figure 10. UKF and UKF-CT estimation results during a slow ramp steer in dry tarmac conditions, with $\mu_{max,0} = 0.7$. The notation 'Meas.' indicates the measurements from the on-board sensors for estimator validation.

Figure 11 refers to a section of the handling circuit with wet tarmac, with $\mu_{max,0}$ purposely set to 1 despite the actual μ_{max} varies in the 0.4–0.7 range, which represents a major initial error in the expected tyre-road friction condition. In this extreme handling scenario, the tyre model approximations lead to inaccuracies that increase process uncertainty. The vehicle speed estimation of the UKF loses reliability in high slip ratio conditions, corresponding to peak values of $|\sigma_{xij}| > 0.2$, occurring in multiple time windows (18–20 s; 23–24 s; 26–28 s; 30–38 s; after 46 s), when the vehicle is subject to hard braking or swift accelerations. In these scenarios the UKF speed estimate presents spikes caused by the loss of relevance of the angular wheel speed measurements, and the need to increase reliance on the acceleration sensors. To cope with these criticalities, examples from the previous literature implemented complex adaptive strategies to vary the filter covariances depending on the expected reliability of the process model or sensors, deduced from the driving conditions [6]. However, in the UKF-CT the presence of the F_{xij} inputs from the smart tyres effectively aids the estimator to cope with high slip ratio conditions, as confirmed by the figure and the low values of σ^{std} of V in Table 2. The utilisation of the smart tyre system permits to safely keep the filter calibration (i.e. the covariances) constant, since also $\hat{\mu}_{max}$ promptly converges to the correct value, and the β estimation KPIs are close

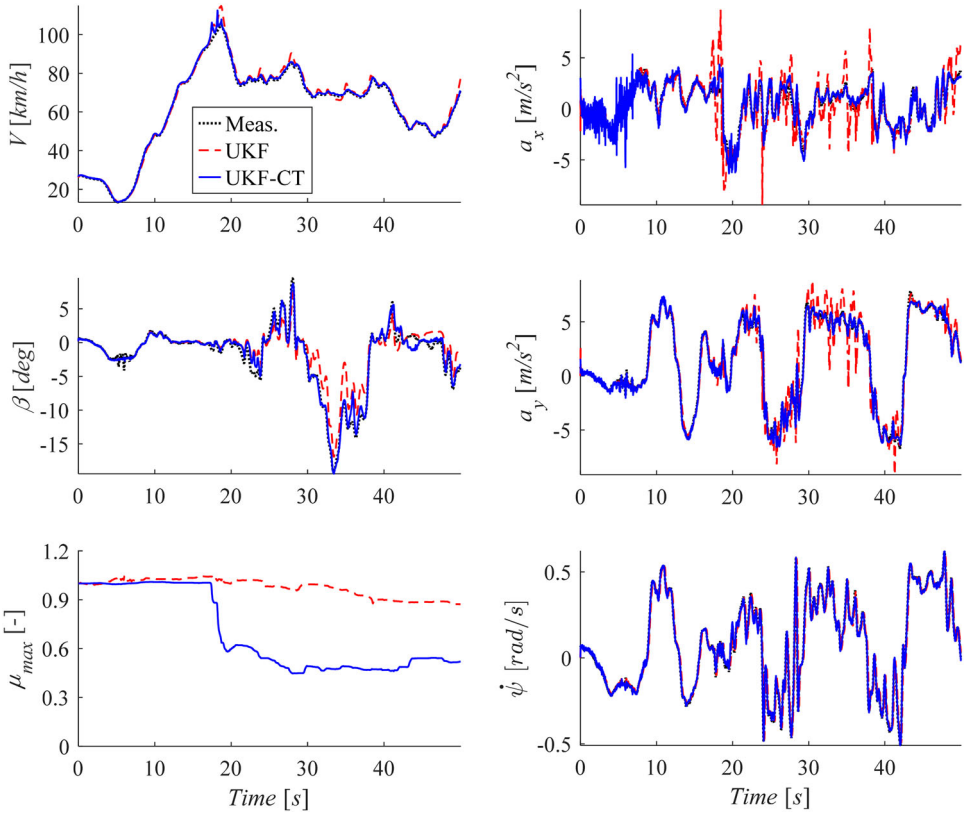

Figure 11. UKF and UKF-CT estimation results during a handling circuit lap in wet tarmac conditions, with $\mu_{max,0} = 1.0$.

to those obtained from correctly initialised friction conditions (which are not shown, but were assessed during the study), or from $\mu_{max,0} = 0.7$, see Table 2.

Finally, Figure 12 shows a step steep on dry tarmac, with $\mu_{max,0} = 1$. In these extreme limit and post-limit handling conditions, the experimental validation of vehicle dynamics model based filters, such as the UKF of this study, tends to be particularly problematic (see the UKF performance in the 4–6 s time window in Figure 12), because of the inevitable model mismatches, uncertainties and disturbances, which exert significant influence on the internal vehicle model response, thus compromising the estimation performance. Some authors, such as Piyabongkarn et al. [39], cope with extreme transients by merging the dynamic model based estimation with the output of kinematic models or estimators, which are independent from vehicle and tyre parameters as they only rely on the IMU outputs, and can provide good estimation during transients, but have poor performance in quasi-steady conditions, because of the inevitable sensor measurement errors and offsets. However, also in the considered extreme step steer, good performance is achieved through the introduction of the force contributions of the smart tyre system of the UKF-CT, without the need for fusion based or adaptive algorithms. The KPIs in Table 2 and Figure 9 confirm that the UKF-CT outperforms the UKF in this test also in the case with $\mu_{max,0} =$

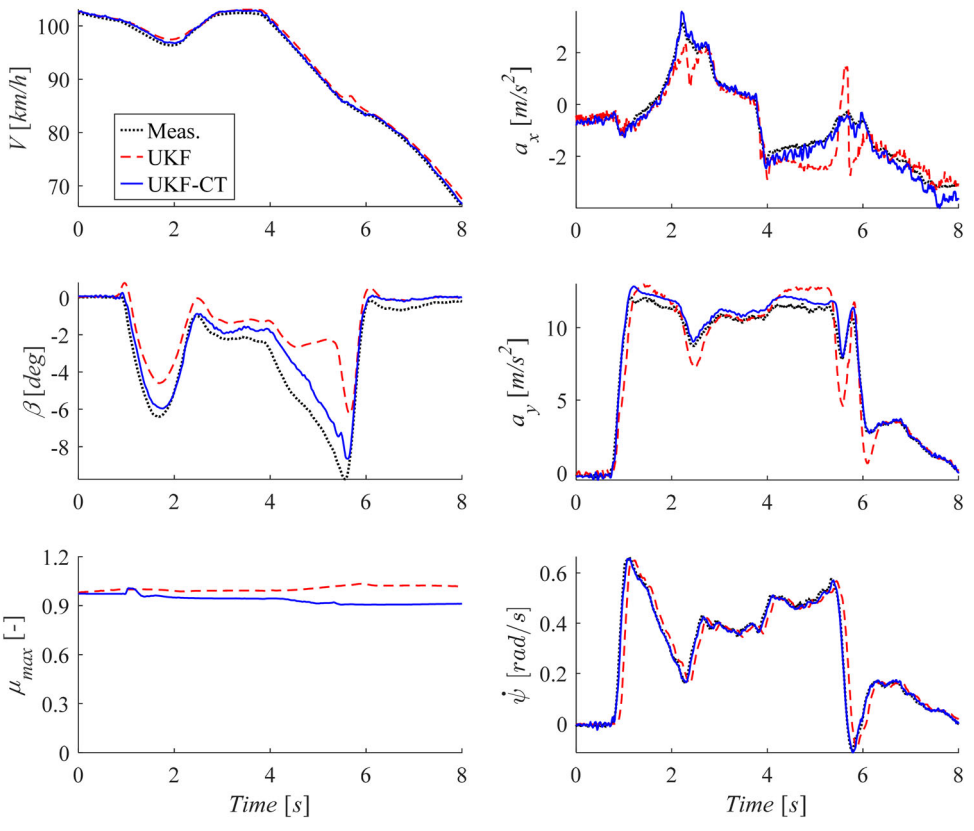

Figure 12. UKF and UKF-CT estimation results during a step steer in dry tarmac conditions, with $\mu_{max,0} = 1.0$.

0.7, due to the better convergence properties of the RWM assisted by the tyre force feedback.

4.3. Robustness analysis

Model based state estimators often use internal vehicle models with time-invariant parameters, referred to nominal conditions, and thus neglect phenomena like the variations of: (i) vehicle mass, e.g. caused by the number of passengers, payload, and fuel; (ii) position of the centre of gravity; and (iii) tyre parameters, e.g. provoked by tyre replacements or wear.

The tyre ID function of the considered smart tyre system provides the information on the installed tyre model, which already represents significant progress with respect to a conventional solution, as the tyre parameters of the state estimator can be updated based on the installed tyres. Moreover, as discussed in Section 3, see (19)-(20), the availability of the tyre contact forces from the smart tyre system allows periodic updates of the vehicle mass as well as the longitudinal and lateral positions of the centre of gravity. Even more importantly, the continuous tyre force information provided to the UKF-CT intrinsically increases its robustness.

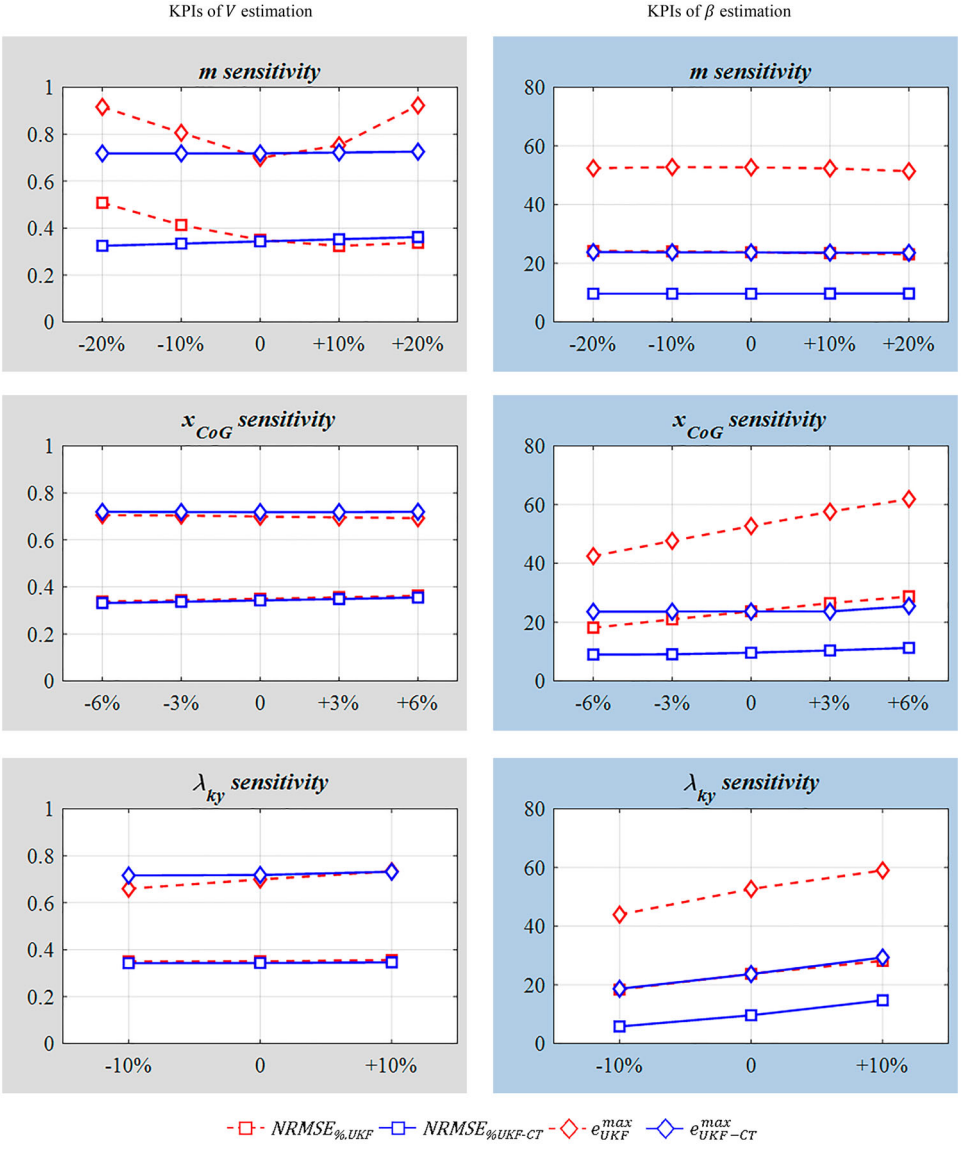

Figure 13. Sensitivity analysis of the UKF and UKF-CT with $\mu_{max,0} = 1$.

This section evaluates the UKF and UKF-CT performance along the SRS manoeuvre, under the assumption of vehicle and tyre parameter uncertainties. Given the availability of experimental measurements from the real vehicle demonstrator, and the obvious difficulty in systematically changing the test vehicle parameters, the robustness analysis is performed by varying individual parameters of the internal vehicle model of the filters, and by comparing the estimation outputs with the experimental measurements in nominal vehicle conditions.

In particular, the involved parameters are: (i) the total vehicle mass, m, which is varied from −20% to +20% with respect to its nominal value; (ii) the longitudinal position of the

centre of gravity, expressed through the normalised coordinate $x_{CoG} = 100\Delta l_R/l$, which is varied from −6% to +6%, where Δl_R is the difference between the rear semi-wheelbase in the internal model and its value on the vehicle prototype; and (iii) the scaling factors of the tyre cornering stiffness in the Pacejka Magic Formula, λ_{ky}, which are simultaneously varied for all tyres from −10% to +10% with respect to their nominal values.

Figure 13 reports the results for the UKF and UKF-CT in terms of $NRMSE_{\%}$ and e^{max} of vehicle speed and sideslip angle. In general, the speed estimation results of the two filters are comparable, even if the UKF shows higher sensitivity to the variation of mass, which is detected by the UKF–CT in the initial section of the manoeuvre. With respect to β, the vehicle mass variations do not affect the sideslip angle estimation performance of either filter, while only the UKF is sensitive to the variation of the longitudinal position of the centre of gravity, which is recognised by the UKF-CT through the automated update function in (20), and both filters are sensitive to cornering stiffness variations. The clear outcome of the analysis is that the UKF-CT is consistently better in estimating β than the UKF, and brings more than halved $NRMSE_{\%}$ and e^{max} values for any considered parameter variation.

5. Conclusions

The paper dealt with a novel estimator, i.e. the UKF-CT, of the key dynamic states for vehicle dynamics control. The main feature of the UKF-CT, based on a nonlinear double-track vehicle model with wheel dynamics, is the inclusion in the measurement vector of the longitudinal and vertical tyre forces generated by a smart tyre system. The performance of the UKF-CT was compared with that of a state-of-the-art estimator, i.e. a UKF using the same vehicle model as the UKF–CT but excluding the smart tyre system inputs, along a comprehensive set of handling manoeuvres with different tyre-road friction conditions, carried out with a McLaren 570S vehicle prototype including smart tyres. For fairness of comparison, the estimators were tuned through a genetic algorithm based optimisation routine, using the smart tyre outputs for the calibration of the process covariance matrices of both filters.

The experimental results show that the smart tyre force feedback brings major improvements in terms of: (i) convergence of the estimated tyre-road friction factor to its correct value, which allows reliable sideslip angle and vehicle speed estimation also when the filter is initialised with significant errors with respect to the actual friction conditions; and (ii) state estimation performance during extreme transient manoeuvres at the limit and beyond the limit of handling, in which the filter without smart tyre information shows the typical limitations of state estimators based on vehicle dynamics models. In terms of performance indicators, the UKF-CT brings an average reduction of the normalised root mean square estimation error ($NRMSE_{\%}$) of vehicle speed by 46% and 73%, and an average decrease of the $NRMSE_{\%}$ of β by 49% and 26%, for the two considered initialisation values of the tyre-road friction condition, in comparison with the UKF without smart tyre inputs. Similarly, for the same tests and two initial conditions of the tyre-road friction factor, the average reduction of the maximum vehicle speed estimation error enabled by the smart tyre system amounts to 39% and 59%, while the maximum sideslip angle estimation error decreases by 33% and 12%. The sensitivity analysis to investigate the influence of the

vehicle and tyre parameters on the estimation performance confirmed the superiority and robustness of the UKF–CT, especially in terms of sideslip angle estimation.

The important conclusion is that for the considered vehicle the UKF-CT provides an overall reliable and robust performance for a wide range of manoeuvres, covering sub-limit, limit and post-limit handling, hard acceleration and braking while cornering, quasi-steady-state and transient conditions, without requiring the adoption of complex process covariance adaptation algorithms, which would be required by the UKF.

Disclosure statement

No potential conflict of interest was reported by the author(s).

Funding

The author(s) reported there is no funding associated with the work featured in this article.

ORCID

Patrick Gruber http://orcid.org/0000-0003-1030-6655
Aldo Sorniotti http://orcid.org/0000-0002-4848-058X

References

[1] Song CK, Uchanski M, Hedrick JK. Vehicle speed estimation using accelerometer and wheel speed measurements. SAE Tech. Pap., no. 2002-01-2229, 2002.
[2] Xiong L, Xia X, Lu Y, et al. IMU-based automated vehicle slip angle and attitude estimation aided by vehicle dynamics. Sensors. 2019;19(8):1930.
[3] Reina G, Paiano M, Blanco-Claraco JL. Vehicle parameter estimation using a model-based estimator. Mech Syst Signal Process. 2017;87:227–241.
[4] van Aalst S, Naets F, Boulkroune B, et al. An adaptive vehicle sideslip estimator for reliable estimation in low and high excitation driving. IFAC-PapersOnLine. 2018;51(9):243–248.
[5] Li X, Xu N, Li Q, et al. A fusion methodology for sideslip angle estimation on the basis of kinematics-based and model-based approaches. Proc Inst Mech Eng Part D J Automob Eng. 2020;234(7):1930–1943.
[6] Li L, Jia G, Ran X, et al. A variable structure extended Kalman filter for vehicle sideslip angle estimation on a low friction road. Veh Syst Dyn. 2014;52(2):280–308.
[7] Doumiati M, Victorino AC, Charara A, et al. On-board real-time estimation of vehicle lateral tire-road forces and sideslip angle. IEEE/ASME Trans Mechatronics. 2011;16(4): 601–614.
[8] Antonov S, Fehn A, Kugi A. Unscented Kalman filter for vehicle state estimation. Veh Syst Dyn. 2011;49(9):1497–1520.
[9] Heidfeld H, Schünemann M, Kasper R. UKF-based State and tire slip estimation for a 4WD electric vehicle. Veh Syst Dyn. 2019;58(10):1–18.
[10] Wielitzka M, Busch A, Dagen M, et al. Unscented Kalman filter for state and parameter estimation in vehicle dynamics. Kalman Filters-Theory Adv Appl, InTech. 2018: 56–75.
[11] Wan EA, Van Der Merwe R. The unscented Kalman filter for nonlinear estimation. Adaptive systems for signal processing, communications and control symposium; 2000. p. 153–158.
[12] Wenzel TA, Burnham KJ, Blundell MV, et al. Dual extended Kalman filter for vehicle state and parameter estimation. Veh Syst Dyn. 2006;44(2):153–171.
[13] Liao YW, Borrelli F. An adaptive approach to real-time estimation of vehicle sideslip, road bank angles, and sensor bias. IEEE Trans Veh Technol. 2019;68(8):7443–7454.
[14] Bechtoff J, Koenig L, Isermann R. Cornering stiffness and sideslip angle estimation for integrated vehicle dynamics control. IFAC-PapersOnLine. 2016;49(11):297–304.

[15] Braghin F, Brusarosco M, Cheli F, et al. Measurement of contact forces and patch features by means of accelerometers fixed inside the tire to improve future car active control. Veh Syst Dyn. 2006;44(sup1):3–13.
[16] Ergen SC, Sangiovanni-Vincentelli A, Sun X, et al. The tire as an intelligent sensor. IEEE Trans Comput Des Integr Circuits Syst. 2009;28(7):941–955.
[17] Sabbioni E, Ivone D, Braghin F, et al. In-tyre sensors induced benefits on sideslip angle and friction coefficient estimation. SAE Tech. Paper, no. 2015-01-1510, 2015.
[18] Singh KB, Taheri S. Estimation of tire–road friction coefficient and its application in chassis control systems. Syst Sci Control Eng. 2015;3(1):39–61.
[19] Cheli F, Leo E, Melzi S, et al. On the impact of 'smart tyres' on existing ABS/EBD control systems. Veh Syst Dyn. 2010;48(S1):255–270.
[20] Singh KB, Arat MA, Taheri S. Literature review and fundamental approaches for vehicle and tire state estimation. Veh Syst Dyn. 2019;57(11):1643–1665.
[21] Nam K, Oh S, Fujimoto H, et al. Estimation of sideslip and roll angles of electric vehicles using lateral tire force sensors through RLS and Kalman filter approaches. IEEE Trans Ind Electron. 2013;60(3):988–1000.
[22] Nam K, Fujimoto H, Hori Y. Lateral stability control of in-wheel-motor-driven electric vehicles based on sideslip angle estimation using lateral tire force sensors. IEEE Trans Veh Technol. 2012;61(5):1972–1985.
[23] Madhusudhanan AK, Corno M, Holweg E. Vehicle sideslip estimator using load sensing bearings. Control Eng. Pract. 2016;54:46–57.
[24] Mazzilli V, et al. On the vehicle state estimation benefits of smart tires. Chassis.tech proceedings; 2020.
[25] Cheli F, Audisio G, Brusarosco M, et al. Cyber Tyre: a novel sensor to improve vehicle's safety. SAE 2011 World Congr. Exhib., no. 2011-01–0990, 2011.
[26] Cheli F, Braghin F, Brusarosco M, et al. Design and testing of an innovative measurement device for tyreroad contact forces. Mech Syst Signal Process. 2011;25(6):1956–1972.
[27] OXTS. RT3000 v3. Available from: https://www.oxts.com/products/rt3000.
[28] Laumann M. Technical customer documentation 0 285 YU0 736, 2019.
[29] BS ISO 8855. Standards publication road vehicles — vehicle dynamics and road-holding ability — vocabulary, 2011.
[30] Pacejka H. Tyre and vehicle dynamics. Oxford: Elsevier; 2005.
[31] Jung S, Kim TY, Yoo WS. Advanced slip ratio for ensuring numerical stability of low-speed driving simulation. Part I: longitudinal slip ratio. Proc Inst Mech Eng Part D J Automob Eng. 2019;233(8):2000–2006.
[32] Kim TY, Jung S, Yoo WS. Advanced slip ratio for ensuring numerical stability of low-speed driving simulation: Part II—lateral slip ratio. Proc Inst Mech Eng Part D J Automob Eng. 2019;233(11):2903–2911.
[33] Nielsen L, Kiencke U. Automotive control systems: for engine, driveline, and vehicle. Berlin: Springer; 2000.
[34] Haykin S. Kalman filtering and neural networks. New York (NY): John Wiley & Sons, Inc; 2001.
[35] Welch G, Bishop G. An Introduction to the Kalman Filter. 2006. p. 127–132.
[36] Julier SJ, Uhlmann JK. New extension of the Kalman filter to nonlinear systems. Signal Process Sens Fusion, Target Recognit VI. 1997;3068:182–193.
[37] ISO 7401. Road vehicles – lateral transient response test methods – Open-loop test methods, 2011.
[38] Grip HF, Imsland L, Johansen T, et al. Vehicle sideslip estimation: design, implementation, and experimental validation. IEEE Control Syst Mag. 2009;29(5):36–52.
[39] Piyabongkarn D, Rajamani R, Grogg JA, et al. Development and experimental evaluation of a slip angle estimator for vehicle stability control. IEEE Trans Control Syst Technol. 2009;17(1):78–88.